# Star polymers: A study of the structural arrest in the presence of attractive interactions

F. Lo Verso,[1,*] L. Reatto,[1] G. Foffi,[2] P. Tartaglia,[2] and K. A. Dawson[3]
[1]*Istituto Nazionale di Fisica della Materia and Dipartimento di Fisica, Università di Milano, Via Celoria 16, I-20133 Milano, Italy*
[2]*Dipartimento di Fisica and INFM Center for Statistical Mechanics and Complexity, Università di Roma La Sapienza, Piazzale Aldo Moro 2, I-00185 Rome, Italy*
[3]*Irish Center for Colloid Science and Biomaterials, Department of Chemistry, University College Dublin, Belfield, Dublin 4, Ireland*
(Received 30 July 2004; published 22 December 2004)

Simulations and mode-coupling theory calculations, for a large range of the arm number $f$ and packing fraction $\eta$ have shown that the structural arrest and the dynamics of star polymers in a good solvent are extremely rich: the systems show a reentrant melting of the disordered glass nested between two stable fluid phases that strongly resemble the equilibrium phase diagram. Starting from a simple model potential we investigate the effect of the interplay between attractive interactions of different range and ultrasoft core repulsion, on the dynamics and on the occurrence of the ideal glass transition line. In the two cases considered so far, we observed some significant differences with respect to the purely repulsive pair interaction. We also discuss the interplay between equilibrium and nonequilibrium phase behavior. The accuracy of the theoretical tools we utilized in our investigation has been checked by comparing the results with molecular dynamics simulations.

DOI: 10.1103/PhysRevE.70.061409 PACS number(s): 82.70.Dd, 64.70.Pf, 61.20.Ja, 61.25.Hq

## I. INTRODUCTION

When a substance dissolves into another to form a true solution and the units dispersed through the solvent are much larger in size than the solvent molecules, we call it a colloidal dispersion. There are different classes of colloidal suspensions: molecules individually larger than 1 nm [1], e.g., proteins, polysaccharides, polymers, as well as dispersions that arise when a number of small molecules associate together to form an aggregate; it is known, for example, that amphiphilic molecules in a suitable solvent, above a critical concentration, can aggregate in micelles [2]. Varying the interactions between the mesoscopic constituent particles in colloidal dispersions results in a broad range of equilibrium and nonequilibrium fluid behavior.

One strategy to study such systems involves summing over the solvent degrees of freedom, leaving an effective interaction between the center of mass of the macroparticles [3]. The resulting effective potential $V(r)$ depends, in a complicated fashion, on the interparticle separation and it is in general state dependent [4,5]. A special example in this context is given by the pair potential describing a star polymer solution.

Star polymers (SP) can be considered as a generalization of polymer-coated colloidal particles in the limit where the number of monomers ($N$) per chain is large and the size of the central core is small with respect to the whole star extension. The repulsive interaction between star polymers at short distances increases very slowly as the interparticle separation decreases, namely in a logarithmic way. The number of chains chemically linked to a core influences the softness of $V(r)$: stars with small arm number $f$ may interpenetrate widely; in the limit case $f=1,2$ the star polymer reduces to a simple polymer chain. Stars with very large $f$ emphasize their colloidal nature, although only in the limit $f\rightarrow\infty$ the potential resembles the hard-sphere one.

Recently, solutions of star polymers have received attention in relation to several medical and industrial applications [6]. Moreover, in the last 10 years, advances in macromolecular chemistry, leading to the synthesis of regular star polymers, have made it possible to explore the physics of very different model systems monodisperse in $N$ and $f$ [7,8]. Finally, these systems are very interesting from a theoretical point of view in relation to their polymer-colloid hybrid character. Indeed the efficient design of new mesoscopic materials with properties intermediate between different classes of colloidal systems is a very important challenge in soft condensed matter physics.

In recent decades the equilibrium and nonequilibrium phase behavior of SP solutions have been widely investigated, both theoretically [9–12] and experimentally [6,13–15]. These systems are an interesting example of a complex fluid for which the phase diagram has special features arising from the ultrasoft nature of the repulsive interaction, e.g., there exists a cutoff value of the functionality $f$ below which the system is fluid for all densities ($f_c=34$) and for $f>f_c$ the phase diagram exhibits several unusual solid lattices as well as reentrant melting [11]; SANS and SAXS experiments on solutions of many-armed stars above $f_c$, e.g., Ref. [16], have revealed different macrocrystal structures as we increase the density. The functionality-dependent bcc and fcc solids [17,18], as well as the reentrant melting transition [19], have been experimentally observed in solutions of starlike block copolymer micelles. A second freezing transition observed in the same experiments can be interpreted as the freezing in a bco crystal [20].

The dynamical properties of star polymers have been extensively investigated. Several studies, focused on star polymers or starlike systems in an athermal solvent with different

*Electronic address: federica.loverso@mi.infn.it

 

arm numbers, have shown that it is quite difficult to nucleate a crystal: in many cases, mainly at high functionalities, the solutions display a gelation transition [21–26]. Molecular dynamic (MD) and Brownian dynamic (BD) simulation data for a large range of $f$ and packing fraction $\eta=(\pi/6)\rho\sigma^3$ show that the dynamics of star polymer solutions is extremely rich. In particular the ideal glass transition line, obtained by means of the mode-coupling theory (MCT) [27], displays a nonmonotonic behavior as a function of $\eta$ and $f$. This behavior has been connected to the $\eta$ and $f$ dependence of the effective hard core diameter of an equivalent hard-sphere (HS) system. The detailed comparison between theoretical predictions and simulations confirms the validity of the MCT approach to study the disordered arrested states in soft matter like colloids [28,29] and in ultrasoft systems like star polymer solutions [30]. In particular it has been confirmed that the modified hypernetted chain integral equation (MHNC) is a very good approximation to study static correlations in systems described by ultrasoft interactions not only in equilibrium [31] but also in metastable states [30].

Recently, a model potential has been suggested to describe SP solutions where, in addition to the excluded volume effects, attraction emerges due to dispersion or depletion forces. For this model the fluid-fluid phase diagram has been determined [31] using mean field theory and two fluid-state theories, MHNC and the hierarchical reference theory (HRT) [32–34] for different $f$. This analysis shows that when the strength of the interaction is strong enough a fluid-fluid phase transition appears but the density-temperature coexistence curve bifurcates at a triple point into two lines of coexistence terminating at two critical points. This peculiar phase behavior is related to the unusual form of the repulsive contribution.

Moreover, it has been shown that self-organized structures, resulting from telechelic linear homopolymers and copolymers, similar to star polymers, can bridge by producing an effective attractive interaction leading to reversible aggregation of macromolecules [35]. These micelles are constituted by telechelic associative polymers which have the associating groups at the chain ends. Above a critical concentration the end groups associate in multiplets, forming flowerlike polymeric micelles. At higher concentrations the process of bridging can lead to the formation of a transient gel or also induce macroscopic phase separation [36,37].

The aim of this paper is to investigate the effect of attractive interactions on the dynamics and on the occurrence of the ideal glass transition line, trying to emphasize the special features of the phase behavior arising from the ultrasoft nature of this repulsive effective interaction. We also qualitatively discuss the interplay between equilibrium and nonequilibrium phase behavior. In this work different theoretical and numerical methods have been utilized (mean field theory, fluid state theories, mode-coupling theory, molecular dynamic simulations).

We recall that in recent years a great number of studies have focused on the dynamical behavior of short ranged attractive systems, which are characterized by a strong repulsive core besides the attraction. In particular, when the range of the attraction becomes much shorter than the typical diameter of the colloids, phenomena like a reentrant glass transition or the existence of two different glassy phases emerge [38–40]. This peculiar behavior has been confirmed by a large number of simulations [41–44] and experiments [45–47]. Note that, historically, these new findings have been predicted for the first time within MCT calculation and only on a second stage confirmed by experiments. Consequently it is clear that this kind of approach can be extremely useful also for different interaction models. It is interesting now to focus the attention on ultrasoft repulsion (typical, for example, of a SP solution) and an attraction with different range (which could be typical, for example, of depletion interactions) and to investigate the possibility of new features.

This paper is organized as follows. In Sec. II we present the general framework for our research. In particular, in Sec. II A we introduce the interaction model we chose to study star polymers in presence of attraction. Then in Secs. II B–II D we describe the theoretical and numerical tools we used to study the structural properties, the structural arrest, and the diffusivity in dense star polymer solutions: MHNC, MCT, and MD, respectively. In particular we discuss the application of the modified hypernetted chain integral equation to study the structural properties of star polymer solutions and some test of its accuracy when attractive interactions are taken into account in addition to the entropic contribution.

In Sec. III we consider the effect of attraction on the slow dynamics and structural arrest of star polymer solutions. We carried out a mode-coupling theory analysis which allows us to locate the nonergodicity transition curve of the system, using as input the information on the structure obtained by MHNC. Our aim is to complete the picture of the phase diagram of a star polymer solution in the presence of attractive forces, investigating the dynamics, for the values of the parameters which govern the intensity of the attraction extensively discussed in Ref. [31]. Then we modify these parameters in such a way as to consider attractive forces of shorter range, and we focus on the effect of these modifications on the properties of the glass state. In order to test this difference, molecular dynamics simulations have been performed and the diffusivity of the SP fluid has been evaluated up to crystallization. In this section we again discuss the structure of the system very close to the glass phase.

Finally, in Sec. IV we discuss and summarize our results and we draw our conclusions.

## II. INTRODUCTION TO THE MODEL AND METHODS OF STUDY

### A. Effective pair interaction

The effective pair interaction between star polymers with $f$ arms in a good solvent is purely repulsive and for $f \geqslant 10$ it reads as follows:

$$\frac{V_{\mathrm{rep}}(r)}{k_BT} = \frac{5}{18}f^{3/2}\left[-\ln\left(\frac{r}{\sigma}\right)+\left(1+\frac{\sqrt{f}}{2}\right)^{-1}\right] \quad (r \leqslant \sigma)$$
$$= \frac{5}{18}f^{3/2}\left(1+\frac{\sqrt{f}}{2}\right)^{-1}\left(\frac{\sigma}{r}\right)\exp\left[\frac{-\sqrt{f}(r-\sigma)}{2\sigma}\right] \quad (r>\sigma), \tag{1}$$

where $\sigma$ is the corona diameter of the star and depends on

the number $N$ of monomers of a single arm [48]. Witten and Pincus determined by scaling theory the explicit form of such interaction at short distances [9]; it has been also shown that the good agreement between theory and experiments significantly improves if the model interaction has, in addition to a logarithmic repulsive core, a long range interaction of Yukawa form [10,15,49,50]. This model interaction gives a good description of small angle neutron scattering (SANS) results on concentrated star polymer samples [15] for an wide range of $f$ values. For $f \leqslant 10$ a logarithmic-Gaussian potential more accurately describes the effective interaction [51] but we do not study this regime.

In a previous paper [31] the phase diagram of star polymer solutions was investigated when the effective interaction between two star polymers contains an additional attractive contribution $w(r)$ to be added to the repulsive part $V_{\mathrm{rep}}(r)$ of equations (1):

$$V_{\mathrm{tot}}(r) = V_{\mathrm{rep}}(r) + w(r). \tag{2}$$

This attraction could stem, for example, from a van der Waals interaction arising from a nonperfect matching between the refraction index of the solvent and of the polymer in a way that does not alter the basic configuration of the single star polymer; in this case $w(r)$ is independent from the temperature. Alternatively attraction could be induced by depletion interaction when a third component, which is large compared with the solvent molecules but small compared with the star polymers, is present in the solution. In this case $w(r)$ has an entropic origin and consequently it depends on $T$. In this situation the size and concentration of the depletant are, respectively, closely tied to the range and strength of the attraction. In what follows we shall use temperature as control parameter.

To study the structural arrest and the dynamics in the presence of attractive forces we can use the simplified model potential utilized in Ref. [31] where $w(r)$ has the functional form of a Fermi distribution, i.e.,

$$w(r) = -\frac{C}{\exp\left[\dfrac{r-A}{B}\right] + 1}. \tag{3}$$

The parameters $A$ and $B$ control the position and the width of the well potential, $C$ is the amplitude of the attractive contribution. For convenience we use reduced units for temperature in terms of $C$: $T^* = k_B T/C$. By a suitable choice of these parameters one can guarantee, for the temperatures of interest, that $V_{\mathrm{tot}}(r)$ does not have a significant subsidiary maximum at large $r$ and avoid possible complications due to the competition over different length scales. We have studied three sets of parameters $A$ and $B$ in order to see the dependence of the glass transition on the range and the width of the attractive well. The first case corresponds to the potential discussed in Ref. [31], i.e., $A=2.1\sigma$, $B=0.35\sigma$ and we refer to this case as $SP_1$. For these values of the parameters, the attractive contribution is rather long ranged and we found that $w(r)$ does not modify the ideal glass transition with respect to the purely repulsive case. For the other two choices of the parameter, $SP_2$ corresponding to $A=1.95\sigma$ and $B=0.21\sigma$ and $SP_3$ corresponding to $A=1.875\sigma$ and $B=0.155\sigma$ the attractive well is displaced to smaller distance and we observed significant differences for the glass transition with respect to the only repulsive pair interaction. In Fig. 1 we show the shape of the potential in the three cases for $f=50$. It should be noticed that due to the ultrasoft character of $V_{\mathrm{rep}}$ the value of $A$ and $B$ modifies not only the range of the interaction and the position of the minimum but also the depth of the well potential. In addition, the position and width of the attractive well depends on temperature because $V_{\mathrm{rep}}$ scales with $T$. In Fig. 1 we plot also $V_{\mathrm{rep}}$, at short distances we can observe that $V_{\mathrm{tot}}$ is softer than $V_{\mathrm{rep}}$.

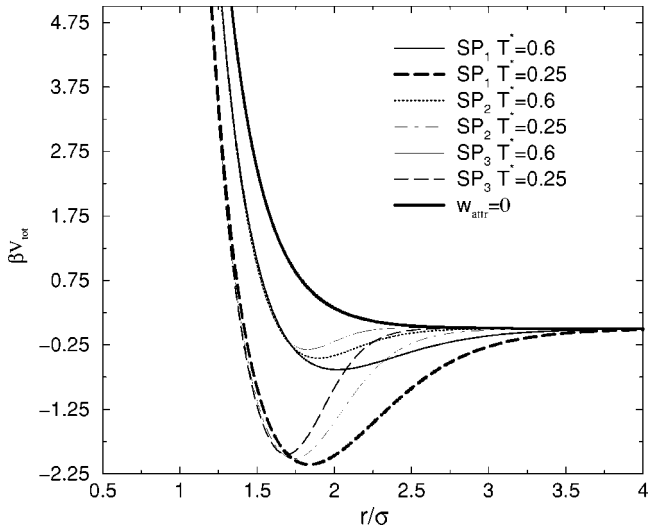


FIG. 1. $\beta V_{\mathrm{tot}}(r)$ versus the interparticle separation $r/\sigma$ for two different temperatures and $f=50$; $T^* = k_B T/C$. We call $SP_1$ the interaction studied in Ref. [31], i.e., $A=2.1\sigma$, $B=0.35\sigma$; $SP_2$ the interaction corresponding to $A=1.95\sigma$ and $B=0.21\sigma$; finally, $SP_3$ corresponds to $A=1.875\sigma$ and $B=0.155\sigma$. The figure also shows $V_{\mathrm{rep}}$ corresponding to $f=50$.

### B. Modified hypernetted chain integral equation

In the present work we carry out a mode-coupling theory (MCT) analysis [27] of the long-time limit of the correlation functions to locate the ideal glass transition line of the system. MCT provides a set of closed equations to calculate the nonergodicity parameter $f_q$ which acts as an order parameter for the glass (see Sec. II D). All the information needed to solve these equations is contained in the static structure factor, defined as $S(q) = \langle \rho(-q)\rho(q) \rangle / N$ and in the number density, $\rho = N/V$, $\rho(q)$ being the density fluctuation variable of wave vector $q$. To calculate $S(q)$, we utilized the MHNC integral equation. This equation is in general accurate also when an attractive contribution to the interaction is present [52]. In the case of star polymers in a good solvent it has been verified the remarkable accuracy of this theory, to describe fluid states as well as metastable states [30,31] for a large range of $f$ and density values.

The starting point for the MHNC equation is an exact relation [53], obtained from a cluster expansion, which con-

nects the radial distribution function (rdf) $g(r)$ to the interparticle potential $V(r)$,

$$g(r) = \exp[-\beta V(r) + h(r) - c(r) + E(r)], \tag{4}$$

where $h(r)=g(r)-1$ and $c(r)$ are the pair and the direct correlation function, respectively. $c(r)$ is related to $h(r)$ by the Ornstein-Zernike equation.

The term $E(r)$, called bridge function, represents a sum of an infinite number of terms, the so-called elementary graphs in the diagrammatic analysis of the two-point function and, in general, it is not known. In the MHNC scheme the $E(r)$ is replaced by the bridge function of a fluid of hard spheres, $E_{\mathrm{HS}}(r)$, of suitable diameter $d$. To optimize this choice, which depends on the parameter $d$, the free energy is minimized [54]. This is equivalent to satisfy the relation

$$\int d\mathbf{r}[g(r) - g_{\mathrm{HS}}(r, \eta_{\mathrm{HS}})]\frac{\partial E_{\mathrm{HS}}(r, \eta_{\mathrm{HS}})}{\partial \eta_{\mathrm{HS}}} = 0 \tag{5}$$

where $\eta_{\mathrm{HS}}=(\pi/6)\rho d^3$.

In order to implement MHNC one needs the rdf $g_{\mathrm{HS}}(r)$ of hard spheres from which one can obtain $E_{\mathrm{HS}}$. Verlet and Weis (VW) [55] provided an accurate parametrization of $g_{\mathrm{HS}}(r)$ based on the PY equation with a correction which incorporates thermodynamical consistency through the Carnahan-Starling state equation [53]. This together with equations (4) and (5) gives a closed set of equations which are solved by a standard iterative method.

In a previous paper some of the authors showed that the dependence of $\eta_{\mathrm{HS}}$ on the density as determined by Eq. (5) is unusual and reflects the features of the interparticles interaction [31]. Moreover, in Ref. [30] we found evidence that the characteristic sequence of maxima and minima of $\eta_{\mathrm{HS}}$ versus $\eta$ is directly related to the nonmonotonic behavior of the diffusion coefficient as a function of the packing fraction. Indeed the slow dynamics in star polymer systems at low and intermediate densities can be qualitatively described as the slow dynamics of the hard sphere system via a density and functionality dependent effective diameter determined with MHNC closure.

### C. Molecular dynamic simulation: comparison between MHNC and MD results on the correlations

To check the results of the MHNC and MCT calculations, we performed extensive MD simulations for the model described by the potential defined by Eqs. (1)–(3). We simulate $N=1000$ particles for different values of the density, temperature, and functionality. For each state point the configurations have been equilibrated at constant temperature for a time long enough to ensure both the equilibration and decorrelation from the initial configuration. The acquisition run started after this preliminary preparation, then the system was simulated at constant energy. We carefully checked whether crystallization occurred or not during the run by inspection of the static structure factor, with the same modulus, not averaged over different directions of $q$ vectors. In fact to improve the averages in the calculations of $S(q)$ at a given $q$, we generally considered up to 300 independent $q$ vectors chosen with a random direction but with the same modulus $q$. In correspondence of these values, we evaluated the density variables and consequently the static structure factor for a given direction. Finally, we averaged on the different directions. For a liquid the structure is extremely disordered and all the terms for different directions give roughly the same contribution to the average. When the structure factor corresponding to a certain direction starts to grow over the others, the system begins to show a preferable direction, i.e., crystallization takes place. When a configuration crystallized we discarded it. As discussed for the purely repulsive case [30], the system has a strong tendency to crystallize, being monodisperse in diameter [44]. Consequently, we will test our predictions only when the system remains in the liquid phase, a future direction of our research may be directed toward the suppression of crystallization introducing, for example, a second component slightly different in diameter [44]. We chose as unit of length the corona diameter $\sigma$ and as unit of mass the mass of the particles. Moreover, we measure the temperature in reduced units, i.e., $T^*=k_BT/C$.

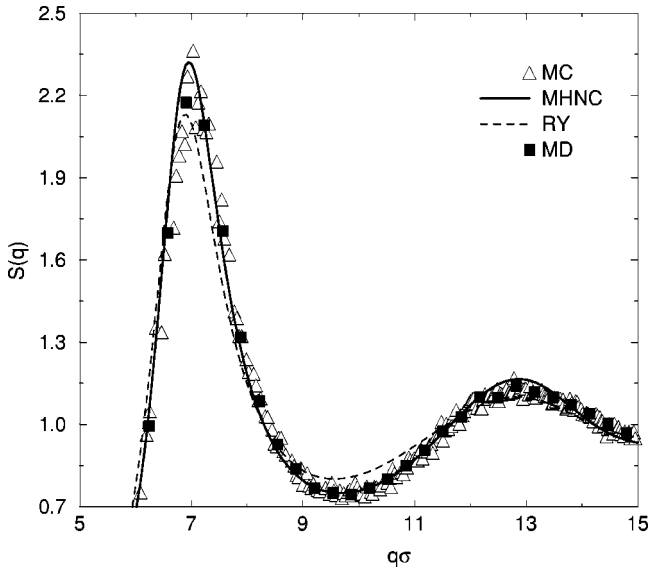


FIG. 2. Athermal solvent: comparison between the main peak of the structure factors we obtained with MHNC closure and MD simulation with the results obtained by Watzlawek *et al.* by means of MC simulation and RY closure; $\eta=0.60$, $f=32$ [$S(q)$ versus $q\sigma$].

We begin our discussion on the numerical simulation by discussing the purely repulsive case, i.e., $C=0$. As extensively described in Ref. [31], MHNC gives a very accurate description of correlations for star polymers in a good solvent for a wide range of densities. In Fig. 2 we present results for the repulsive case, for $f=32$ and $\eta=0.6$ obtained from MHNC and Rogers-Young (RY) theoretical calculations and from MC and MD simulations [56]. The RY equation is another integral equation for $g(r)$ which interpolates between PY and HNC equations [57]. The agreement between MD and MHNC, and between MD simulations and MC simulations, is extremely good. The small apparent MD underestimation of the main peak is due to the grid we used in the simulations. A more refined grid, however, would increase the noise in the data. On the other hand, RY shows

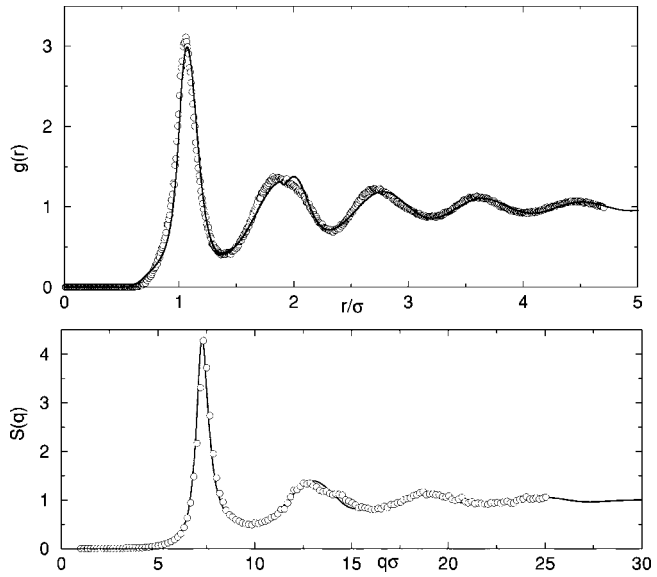


FIG. 3. Comparison between the radial distribution function (top) and the structure factor (bottom) we obtained with the MHNC closure (solid line) and MD simulation (opaque circles); $\eta=0.628$, $T^*=0.25$, $f=50$, $SP_2$.

some significant discrepancies with respect to simulations results in the range of strong coupling which emerges for packing fractions of order of $\eta=0.60$ and $\eta=3$ [31]. By comparison with simulation results (both MC and MD) we definitively conclude that MHNC describe accurately the structure of star polymers in a good solvent.

Hence, we focused on the attractive case and we compare the MD results and the prediction of the MHNC theory for the fluid case: in particular we compared the radial distribution function and the structure factor for the three different models of the attraction described in Sec. II B in a regime of strong coupling when the main maximum of $S(q)$ reaches large values. The temperatures and packing fractions we have chosen in our study correspond to states of interest in the study of the ideal glass transition line, i.e., close to the fluid-glass and glass-fluid ideal transition line. We find in general very good agreement between MD results and MHNC results for all the values of temperature, packing fraction, and arm number investigated. In particular a good accuracy is achieved in the determination of the position of the main peak in the radial distribution functions and structure factors. Only for states at low temperature and at packing fraction corresponding to very large coupling (e.g., see Fig. 3) one notices some small discrepancies between MHNC and MD results.

This analysis confirms the accuracy of the MHNC integral equation in describing the structure of an ultrasoft core potential also in the presence of an attractive contribution at longer range.

One can notice that the MHNC $g(r)$ has some structure in the region of the second maximum and this can even show up as a subsidiary maximum (Fig. 3). It is known [52] that this spurious structure is a consequence of the VW parametrization of $g_{\mathrm{HS}}$ in terms of the PY solution but it is believed that this anomaly has no serious consequence in $S(q)$.

### D. Mode-coupling theory for the ideal glass transition

In this section, we shall briefly review the nature of MCT, and discuss the type of information it yields. The MCT of supercooled liquids describes the dynamical transition by a nonlinear integro-differential system of equations for the normalized time correlation functions of density fluctuations $\Phi(q,t)=\langle\rho(-q,t)\rho(q,0)\rangle/\langle\rho(-q,0)\rho(q,0)\rangle$, where $\rho(\mathbf{q},t)=\Sigma_l \exp[i\mathbf{q}\cdot\mathbf{r}_l(t)]$. As discussed above, the only input to the MCT equations is the equilibrium static structure factor, $S(q)$ and the number density, $\rho$. The glass transition can be identified by studying the long time limit of the MCT equations, which determine the nonergodicity parameter of the system $f_q=\lim_{t\to\infty}\Phi(q,t)$. An ergodic state is characterized by $f_q=0$. This value is always a solution of the MCT long-time limit equations [27].

The quantity $f_q$ obeys the equation $f_q/(1-f_q)=\mathcal{F}_q(f)$. Here, the mode-coupling functional $\mathcal{F}_q$ is given by

$$\mathcal{F}_q(f)=\frac{1}{2}\int\frac{d^3k}{(2\pi)^3}V_{\vec{q},\vec{k}}f_k f_{|\vec{q}-\vec{k}|}. \tag{6}$$

Equation (6) together with the equation for $f_q$ can be derived by taking the long-time limit, $t\to\infty$, of the MCT equations [27]. The mode-coupling vertices are determined by the structure factor $S_q$, the direct correlation function $c_q$, and the density $\rho$,

$$V_{\vec{q},\vec{k}}\equiv S_q S_k S_{|\vec{q}-\vec{k}|}\rho[\vec{q}\cdot\vec{k}c_k+\vec{q}\cdot(\vec{q}-\vec{k})c_{|\vec{q}-\vec{k}|}]^2/q^4. \tag{7}$$

The direct correlation function is directly related to the static structure factor by the relation $c_q=(1/\rho)[1-(1/S_q)]$. The glass transition appears as an ergodic to nonergodic transition for the system, where $f_q\neq 0$ solutions arise. These transition points correspond to bifurcation singularities of the MCT equations (6) and (7).

In the present work, we numerically solved Eqs. (6) and (7) with an iterative procedure over a grid of 650 equispaced $q$ vectors up to $q=62.32$. For the static structure factor we used the static MHNC structure factor $S(q)$ calculated as described above.

## III. RESULTS

### A. $SP_1$: MCT and MD results

First of all we considered the model potential we labeled $SP_1$. At low temperature the system has fluid-fluid phase transition with two critical points: the first critical point is around $\eta_c=0.026$ and $T_c^*\simeq 0.7$, the second one around $\eta_c=1.04$ and $T_c^*\simeq 0.156$. Far from the critical point, we observed that the structure factor $S(q)$, relative to the potential $V_{\mathrm{tot}}$, is not very different from the structure factor relative to the simply repulsive interaction $V_{\mathrm{rep}}$. In particular the position of the main peak does not change appreciably and its height change for less than 1% ($0.2\lesssim T^*\lesssim 0.6$). Consequently one might expect that the location of the ideal glass transition will not be different from the repulsive case [30]. Indeed this is the case. We studied several arm numbers (from low value, $f=24$,32 to higher one $f=70$) for several values of the packing fraction with MCT. Similarly to the

case of purely repulsive interaction we deduce that below $f=46$ there is no glass phase. For $46<f<60$ the system is fluid for low densities and glass for intermediate ($0.25\lesssim\eta\lesssim0.7$), but it is still fluid at high densities ($\eta>0.7$). When $60<f<72$ the system is in a glass state for intermediate and very high densities ($0.25\lesssim\eta\lesssim0.7$, $\eta\lesssim2.25$). Finally, above $f\simeq72$ the system is fluid for low densities ($\eta\lesssim0.25$) and in a glass state for intermediate and high densities ($\eta\gtrsim0.25$).

Hence, the effect of the attraction does not change the location of the ideal glass transition. Consequently, in the temperature-packing fraction plane, the ideal glass transition line would be trivially represented by a vertical line.

We also performed molecular dynamic simulations to calculate the dependence of the diffusion coefficient, from the long-time limit of the mean squared displacement, varying the temperature, for different values of $f$ and the packing fraction. This analysis supported the MCT predictions, i.e., the diffusion coefficient does not change appreciably with the temperature.

Starting from the behavior of the structure factor changing the temperature and from the analysis of the structural arrest we performed, we can complete the picture of the phase diagram. For $f\leqslant34$ there is no freezing transition, the two fluid-fluid phase transitions represent stable states; for $f\gtrsim50$ all the density region above the density corresponding to the triple point $T_p$ is occupied by crystalline phases; for $34<f\lesssim50$ the fluid-fluid phase transitions and their critical points persist as stable states. In Fig. 4 we describe the whole phase diagram for $f=50$: the fluid-fluid phase diagram is calculated by means of mean field theory and the ideal glass transition lines determined with MCT. At the equilibrium the region around the second critical point becomes metastable with respect to the freezing, the regions between two successive squares (from low to high densities), in the upper part of the figure, indicate the densities where the system is solid (data are MC results reproduced by Watzlawek *et al.* [11]). If the crystallization can be avoided we can observe that the second critical point lies outside the glassy region (see also the inset). The limit of very high temperatures, i.e., the purely repulsive interaction are also shown in Fig. 4, the densities which delimit the glass region are effectively the same with and without attractive interaction.

We conclude that, varying $f$, the first critical point will always lie outside the glass region. The second critical point, however, will enter the glassy phase for $f\gtrsim70$.

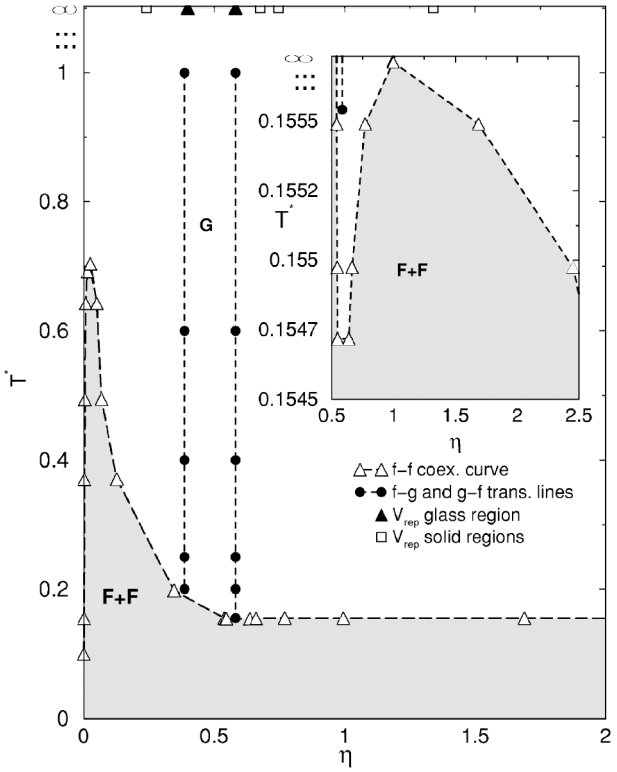


FIG. 4. $SP_1$ fluid-fluid phase diagram (opaque triangles up) for a star polymer solution calculated by means of mean field theory and the ideal glass transition lines (filled circles) determined with MCT, which delimit the region where the system is a glass. The inset shows a magnification of the coexistence curve at higher density [31]. On the top of the main figure we present some results about the purely repulsive interaction, which corresponds to the limit of very high temperature: two successive squares (from low to higher densities) delimit the regions where the system is solid at the equilibrium (by Watzlawek *et al.*, MC simulation [11]); the filled triangles represent the densities which delimit the glass region. Notice that the second critical point survives with respect to the glass transition while the region around the second critical point becomes metastable with respect to the freezing. Moreover, we can observe that the densities which delimit the glass region are effectively the same with and without attractive interaction. Lines are simply a guide to the eye.

### B. $SP_2$: MCT and MD results

As anticipated above we tried to tune the parameters $A$ and $B$ in order to enhance the effect of the attraction on the shape of the glass-transition line. Our aim was to shrink the well and move the minimum of the pair interaction close to sigma.

First of all we consider the parameters $A=1.95\sigma$ an $B=0.21\sigma$ ($SP_2$). As we see in Fig. 1 the well potential in this case is shrunken approximately by 30% with respect to $SP_1$ and the position of the minimum is changed approximatively by 6% ($0.25<T^*<0.6$). If compared to $SP_1$ the depth of the well potential changed from 5% with respect to lower temperature untill approximatively 28% around $T^*=0.6$.

In Fig. 5 we present the occurrence of the glassy phase for different numbers of arms and as a function of temperature. For $f>46$ we can summarize our results as follows: for high temperatures the two ideal-glass lines (fluid glass on the left and glass fluid on the right) tend to the repulsive case [30]. On lowering the temperature, however, a fluid-stabilizing effect sets in, so that the fluid-glass line tends to move to larger values of the density. So in the low density region, roughly below $\eta=0.50$, there is the possibility of the glass melting when lowering the temperature. In this case increasing the temperature, the width of the nonergodicity parameter $f_q$, which is a measure of the inverse of the cage localization length, gets larger (see Fig. 6). Moreover, we observe an increase of $f(q=0)$ lowering the temperature, corresponding to densities closer to the coexistence curve. The effect of the

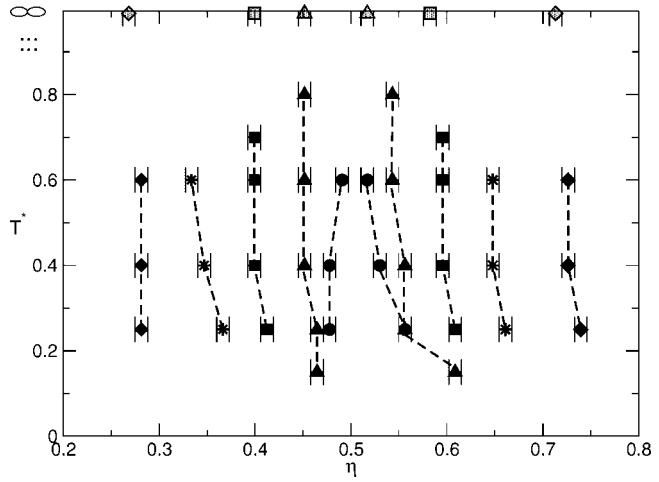


FIG. 5. MCT fluid-glass and glass-fluid lines (computed with MHNC) for different $f$ values and $A=1.95\sigma$, $B=0.21\sigma$ ($SP_2$): reduced temperature $T^*=k_BT/C$ versus reduced packing fraction $\eta=(\pi/6)\rho\sigma^3$. Opaque symbols, circles, triangles, squares, stars, and diamonds correspond, respectively, to $f=45,46,50,58,70$. In the region between two lines, fixed $f$, the system is in a glass phase. The equivalent symbols on the top of the figure delimit the glass regions for $V_{rep}(r)$. We recall that in the limit of $T$ very large we return to the simple repulsive system. Lines are simply a guide to the eye.

attraction for large value of $f$ is very small and in particular for $f=70$ we can see that the fluid-glass line is again very similar to the repulsive case. On the right-hand side of the glass region we can observe that the glass-fluid line moves to higher densities when the temperature decreases and consequently when the intensity of the attraction increases. In contrast to the low density case, the attraction now favors the formation of the glass to higher density with respect to the repulsive case. On lowering the temperature the nonergodicity parameter $f_q$ presents a larger width in $q$. This clearly indicates that the particles are localized on a shorter length scale. This phenomenon could be related either to the effect of a stronger attraction or to a larger value of the effective repulsive length. It is interesting to stress that in all the cases taken into account the nonergodicity parameter, presents the typical shape of a repulsive glass, i.e., a glass that possesses a structure dominated by the caging effect. This typical repulsive behavior is characterized by oscillations in correspondence to the peaks of the static structure factor with a maximum at the first peak. It has been shown, both by MCT calculations [40] and computer simulations [42], that for sufficiently short-ranged attraction, a new glass, which has been named attractive glass, emerges. Indeed the shape of the $f_q$ for an attractive glass is completely different: the oscillations are very weak and the maximum is not so pronounced. In our investigation we encountered fingerprints only of the repulsive glass. The effect of the attraction and the interplay between attraction and repulsion, seem to act more on the size of the cages and on their formation rather than on the nature of the arrest itself. However, we have not investigated the case of very narrow attractive wells on the length scale of $\sigma$.

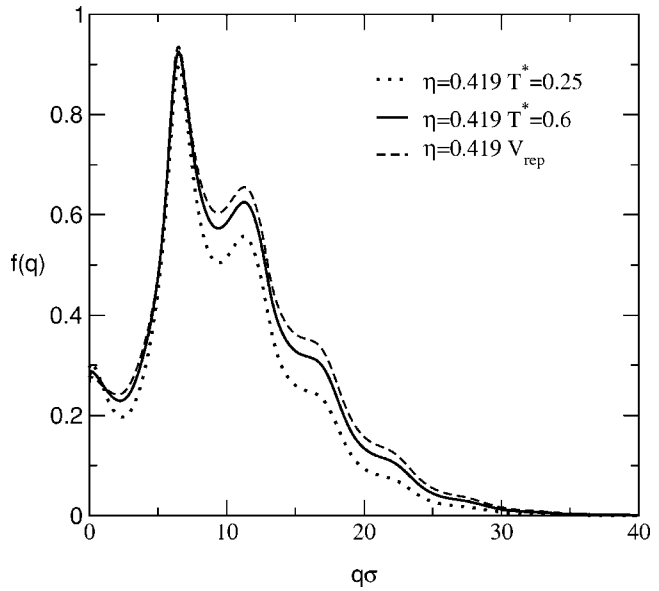


FIG. 6. $SP_2$, nonergodicity parameter $f_q$ versus $q\sigma$ for stars with $f=50$, $\eta=0.8$. Notice the smaller width of this parameter for high temperatures.

The behavior of star polymers with $f=45$ is different: we can observe that the attractive contribution of the interaction favors the occurrence of glass states at low temperature. Indeed for this value of the functionality, a stable glass phase emerges at a temperature $T^*\lesssim 0.6$ from the solution of MCT equations and the density range of the glass phase gets larger on further decrease of the temperature. In this case the $q$ width of $f(q)$ increases lowering the temperature, both for $\eta<0.5$ and $\eta>0.5$. It is interesting to note that no glass transition is found in the corresponding repulsive case, i.e., in the limit of high temperature.

In the so-called "repulsive glasses" the occurrence of the ideal glass transition in the framework of the MCT depends strongly on the behavior of the main peak of the structure factor, i.e., on the first neighbor interactions. In Fig. 7, we can observe a magnification of the main peak of the structure factor for $f=50$ and two different packing fractions on the left-hand side and on the right-hand side of the ideal glass region (MD simulations). For the different temperatures investigated we observe the same trend, for $\eta=0.314$ [Fig. 7(a)] by decreasing the temperature the main peak of the structure factor decreases, showing a loss of the correlation between particles. The opposite trend is observed on the right-hand side, $\eta=0.628$ [Fig. 7(b)]. We also studied the behavior of the first peak in the structure factor for $f=45$, in this case the trend in the glass region is represented by an increase of the main peak lowering the temperature, indeed this effect is responsible for the anomalous formation of the glass at this value of the functionality.

This preliminary and qualitative study, has been supplemented by a more thorough analysis: we performed molecular dynamic simulation for several values of $f$, $T^*$, and $\eta$.

In Fig. 8 we show the diffusion coefficient $D/D_0$ as a function of the temperature calculated for packing fraction not far from the glass region and for different values of $f$ (42, 45, 46, 50). In the present context data for $D$ are normalized by $D_0=\sigma\sqrt{T^*/m}$, in order to take into account the temperature dependence of the microscopic time [44]. The MD-

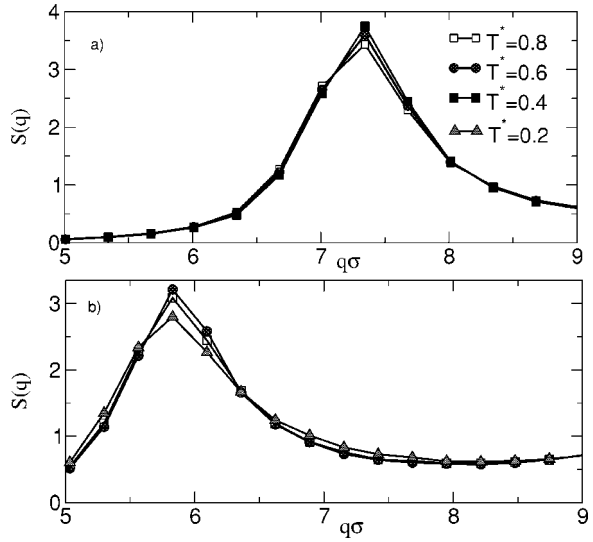


FIG. 7. $SP_2$, $f=50$: magnification of the structure factor (main peak) we obtained with MD simulations at different temperatures. (a) $\eta=0.314$, (b) $\eta=0.628$; $f=50$.

diffusion coefficients as a function of $T^*$ confirm the MCT trend. On the low density side of the glass region the diffusion coefficient decreases, increasing the temperature while on the high density side the diffusion coefficient increases, increasing the temperature. The values of $D/D_0$, for fixed temperature, decrease, increasing $f$; we remark that for $f=42$ the system does not show glass transition.

In general it has been observed that the effect of the presence of a glass transition can be seen as a decrease in the diffusivity also far from that part of the phase diagram where the structural relaxation time starts to grow. Indeed this has been encountered, for example, in a monodisperse square well system [44] and in a purely repulsive soft potential [30]. In MD simulations both these systems presented a strong tendency to crystallize. However, studying the behavior of the diffusivity, it is possible to pin down the shape of the glass transition line. Also in the present work we managed to check that the diffusion follows the MCT predictions. The fact that the $f=45$ trend could not be checked, i.e., an increase of the diffusivity on rising the temperature for both high and low density region, could be related to the fact that the simulations should be run closer to the glass transition and, unfortunately, this is not feasible due to the occurrence of the crystallization. One way around this problem would be to extend the results to a system that presents a smaller crystal nucleation rate. For the square well system, for example, this has been accomplished considering a binary mixture [42].

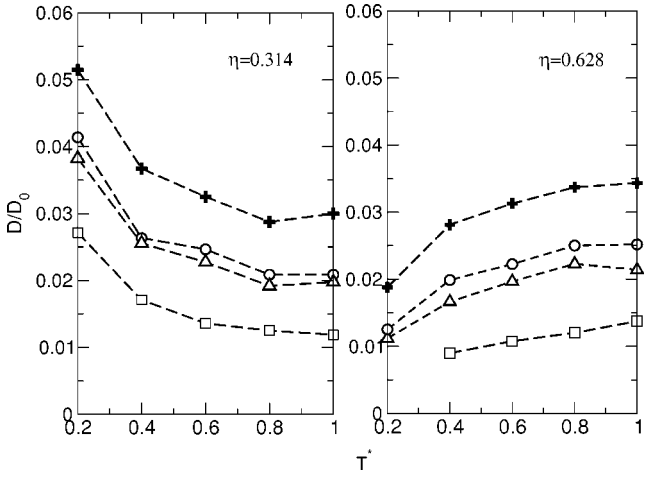


FIG. 8. Reduced diffusion coefficient (MD) for different $f$ values and $A=1.95\sigma$, $B=0.21\sigma$ ($SP_2$). The pluses, circles, triangles, squares, correspond, respectively, to $f=42,45,46,50$ (left panel $\eta=0.366$, right panel $\eta=0.628$). Lines are simply a guide to the eye.

Summarizing, we remark, for the different arm numbers investigated, that for $\eta \lesssim 0.5$ the attraction seems to determine a destabilization of the cages while for $\eta \gtrsim 0.5$ the attraction facilitates the formation of the glass for higher density with respect to $V_{rep}$. The most peculiar behavior has been found for a value of $f$ ($f=45$) for which the glass lines are very near to the value of $\eta=0.5$. For this packing fraction star polymers start to interpenetrate widely. We emphasize that, considering stars in a good solvent at the equilibrium, this value is just in the middle of the bcc ($34<f\lesssim 55$) or fcc ($f>55$) crystal phase. Related to the behavior of the structure factor corresponding to $SP_2$, we expect that also the densities where the system is solid, at the equilibrium, could change weakly with respect to the repulsive case. We will return to this point in greater detail in the conclusions and discussion section.

Finally, we show in Fig. 9 the position of the ideal-glass lines with respect to the fluid-fluid coexistence curves for $f=50$. It turns out that the temperature should be decreased a lot to notice possible effects of the density fluctuations around the second critical point on the ideal glass transition line.

### C. $SP_3$: MCT and MD results

The third case we considered is characterized by $A=1.875\sigma$ and $B=0.155\sigma$, and indicated by $SP_3$. In this case the width of the well potential decreased, with respect to $SP_1$, from approximatively 40% at $T^*=0.25$ until 60% at $T^*=0.6$. The position of the minimum is changed by less than 9%. If compared to $SP_1$ the depth of the well potential changed from 7% with respect to lower temperature until approximatively 48% around $T^*=0.6$.

In Fig. 10 the occurrence of the glass phase is shown for $f=46,50,70$ for a wide range of temperatures. We analyzed in more detail the case $f\leqslant 70$ as here we expect very different behaviors from the three cases in the exam.

For $f\geqslant 50$ the qualitative behavior is very similar to that of $SP_2$. For densities below the glass region the influence of the attractive term, when lowering the temperature, is a liquid-stabilizing effect. In the opposite regime (densities above the glass region), increasing the intensity of the attractive contribution results in moving the glass-fluid line to higher densities with respect to $V_{rep}$. We point out that here the curvature of the lines is more pronounced than in the $SP_2$ case. Anyway, comparing all the cases investigated is not

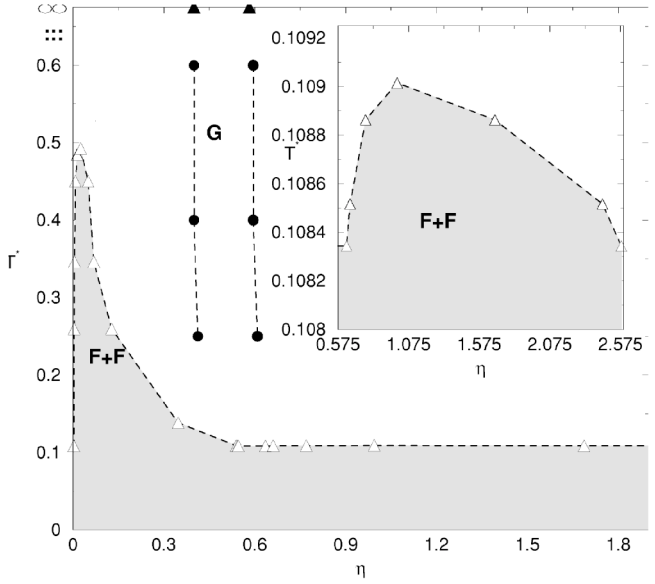


FIG. 9. $SP_2$, fluid-fluid phase diagram for a star polymer solution calculated by means of mean field theory and the ideal glass transition lines determined with MCT. The legend is the same as in Fig. 4. Note that the second critical point survives with respect to the glass transition while the region around the second critical point becomes metastable with respect to the freezing. Moreover, we can observe that decreasing the temperature the densities which delimit the glass region move to higher values (in these cases the effect is small). Lines are simply a guide to the eye.

trivial. This is in part due to the fact that a correct rescaling of the temperature should be done considering the change in the depth and the position of the well potential changing $A$, $B$, and $T$, rather than the amplitude $C$ of the attractive term. We will return to this point in Sec. IV.

For $f \leqslant 46$ the behavior of the star polymer solution is completely different from the previous cases. Indeed for $f=46$ there exists a value of the temperature, $T^* \simeq 0.6$, below which the system does not present a glass transition. For $f=45$ we do not observe any glass phase for all the temperature values investigated ($0.4 \gtrsim T^* \gtrsim 0.8$).

As for the previous case, we performed MD simulations for different arm numbers and temperatures, confirming the MCT result: the trend of $D/D_0$ is qualitatively the same as for $SP_2$ (see Fig. 11). For $f=46$ we do not capture the increasing of the diffusivity when decreasing the temperature, as we expect on the basis of the MCT results on the right-hand side of the glass region. As in the previous case this might be due to the fact that we did not consider packing fractions close enough to the ideal glass lines.

Finally, we studied the behavior of the structure factor, changing the temperature, for $f \leqslant 50$. As for $SP_2$, we calculated $S(q)$ on the left-hand side and on the right-hand side of the ideal glass region (MD simulations).

For $f=50$ the trend is the same as that observed for $SP_2$, i.e., on decreasing the temperature for $\eta=0.314$ the main peak of the structure factor decreases, showing a loss of the correlation between particles. The opposite trend is observed on the right-hand side ($\eta=0.628$).

For $f=46$ the behavior of the structure factor is different. In Fig. 12(a), we present a magnification of the main peak in the structure factor for $f=46$ and $\eta=0.55$ (right-hand side of the glass region). The picture shows a decrease of the main peak of $S(q)$ lowering the temperature. Moreover, in Fig. 12(b) we present a magnification of the main peak in the structure factor for the same arm number and $\eta=0.51$ (left-hand side of the glass region). The trend is exactly the same as for $\eta=0.55$: we stress that, introducing attractive forces, star polymer solutions of 46 arms, show a loss of correlations among particles which are responsible for the peculiar MCT predictions (Fig. 10). This effect is enhanced as the interaction is increased.

Moreover, we also studied the behavior of the structure factor for $f=45$ and $\eta=0.51$; in this case the trend is repre-

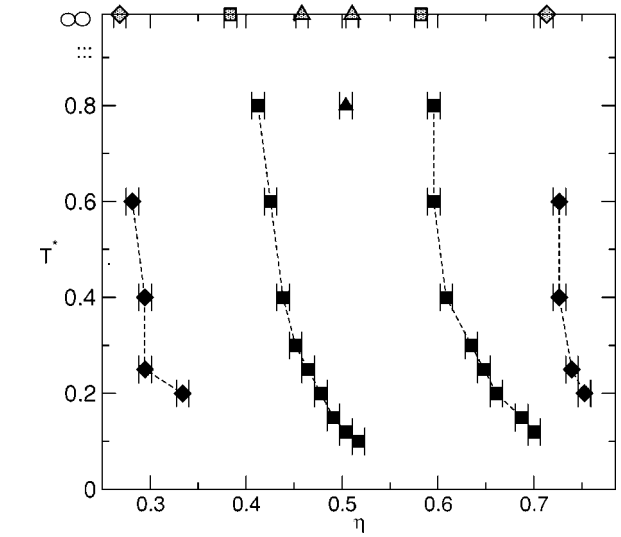


FIG. 10. MCT fluid-glass lines (computed with MHNC) for different $f$ values and $A=1.875\sigma$, $B=0.155\sigma$ ($SP_3$): reduced temperature $T^*=k_BT/C$ versus reduced packing fraction $\eta=\rho\sigma^3$. Filled triangles, squares, and diamonds correspond, respectively, to $f=46,50,70$. The equivalent symbols on the top of the figure delimit the glass region corresponding to $V_{\mathrm{rep}}(r)$. We recall that in the limit of $T$ very large we return to the simply repulsive system.

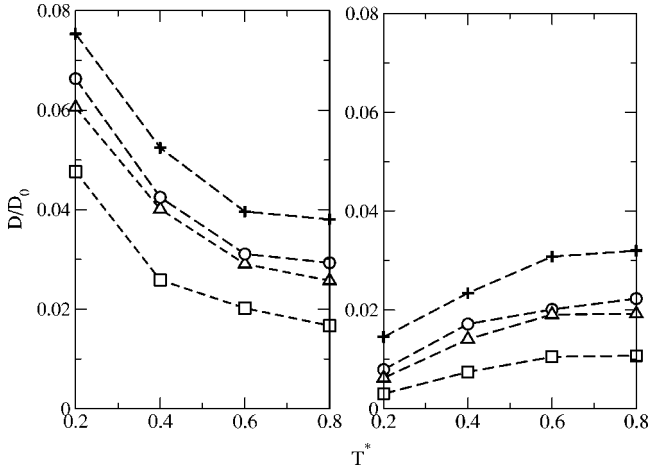


FIG. 11. Reduced diffusion coefficient (MD) for different $f$ values and $SP_3$. The symbols, plus, circles, triangles, squares, correspond, respectively, to $f=42,45,46,50$ (left panel $\eta=0.366$, right panel $\eta=0.628$). Lines are simply a guide to the eye.

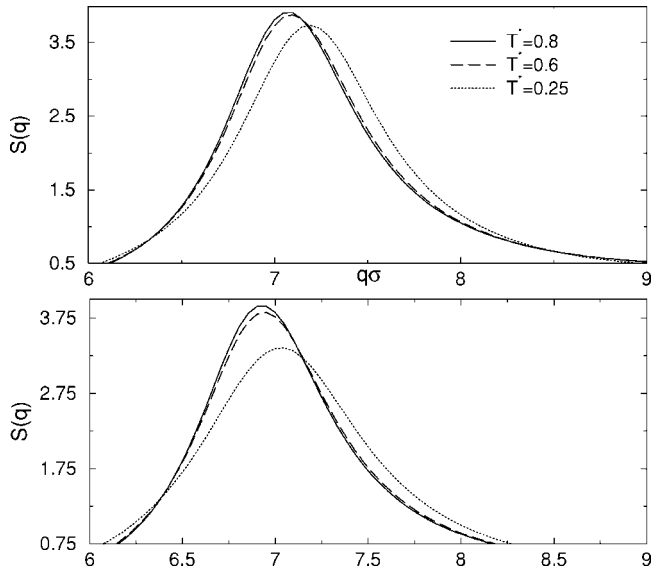


FIG. 12. $SP_3$, $f=46$: magnification of the structure factor (main peak) we obtained with MD simulations at different temperatures. (a) $\eta=0.55$, (b) $\eta=0.51$.

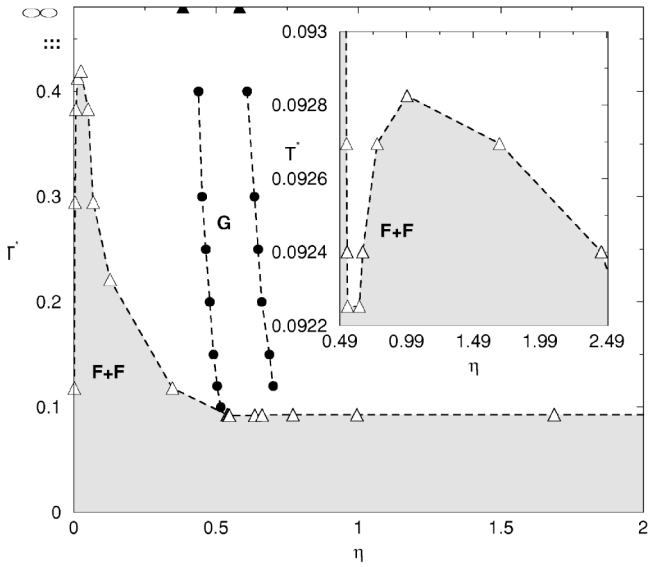


FIG. 13. $SP_3$, fluid-fluid phase diagram for a star polymer solution calculated by means of mean field theory and the ideal glass transition lines determined with MCT. The legend is the same as in Fig. 4. Note that the second critical point survives with respect to the glass transition while the region around the second critical point becomes metastable with respect to the freezing. Moreover, we can observe that by decreasing the temperature the densities which delimit the glass region move progressively to higher values. Lines are simply a guide to the eye.

sented by a decrease of the main peak lowering the temperature. We observed that the height of the main peak introducing the attractive contribution and increasing the intensity of the attraction is in any case smaller than the peak height relative to $V_{rep}$. We recall that for $f=45$, MCT does not give a glass phase for either $V_{rep}$ or $SP_3$.

Summarizing, we can argue from Fig. 10 that for the model interaction $SP_3$ when $\eta \lesssim 0.5$ the attraction always seems to determine a destabilization of the cages, while for packing fractions larger than 0.5 the attraction facilitates the formation of the glass for higher density with respect to $V_{rep}$. For $\eta \simeq 0.5$ (corresponding to the region of interest for $f=46$) the effect of the attraction seems to determine a destabilization of the cages only.

In Fig. 13 we present the fluid-fluid phase diagram and the glass transition lines for $f=50$.

We conclude this section by remarking that, so far, we have discussed only the behavior of the first peak in $S(q)$, while the second peak in the structure factor does not change appreciably in all the cases investigated.

## IV. CONCLUSIONS AND DISCUSSION

In this work, we studied the structural arrest and the dynamics in star polymer solutions when attractive forces between macroparticles are present. The model potential we used to describe the interactions presents an ultrasoft repulsive term of entropic origin at short range plus an attractive interaction at longer range. Due to the addition of the attractive contribution between star polymers the repulsive core becomes softer on lowering the temperature and consequently increasing the intensity of the attraction. We analyzed three different forms of the pair interaction between stars, considering attractive forces of shorter and shorter range. In this paper we focused on stars with several arm numbers (from low value, $f=24,32$ to higher one $f=70$) at several values of density and temperature.

We examined the structure of the solution solving MHNC closure and performing extensive MD simulations, in this way we tested the accuracy of the MHNC to describe the properties which arise from such choice of the interaction model. Over the full range of densities and temperatures of interest MHNC and MD simulations are in a good agreement. Hence we have been able to conclude that MHNC is a good approximation to study systems described by ultrasoft-core repulsive interactions, with and without attractive forces between macroparticles. Having tested the accuracy of the MHNC approach, we focused our attention on the location of the ideal glass transition, studied within MCT.

In particular for the case characterized by the longer range of the attraction, named $SP_1$, the ideal-glass transition line we obtained is not significantly modified in comparison with the one obtained for the purely repulsive potential. Indeed both the structure and the dynamics of the solution are not significantly modified by introducing the attractive contribution. On the other hand, the two other systems characterized by a shorter attractive range show some significant differences with respect to the purely repulsive pair interaction.

For $f \gtrsim 50$ $SP_2$ and $SP_3$, show the same qualitative behavior. In particular we can distinguish two regions in density, a low density regime ($\eta < 0.5$) and a high density regime ($\eta > 0.5$) where the system, in both cases, behaves differently. For low densities, on lowering the temperature, a liquid-stabilizing effect due to the attractive forces sets in, so that the liquid-glass transition line moves to larger values of the density. Indeed, this is an interesting effect since it presents

the possibility of passing from a glass phase to a liquid phase, decreasing the temperature. It is perhaps worth making a few remarks about this issue. It is now well established that systems characterized by a step repulsion and a short range attraction, possess a reentrance in the the dynamical arrest. In these systems it is possible to melt the glass by lowering the temperature. This is a phenomenon now well established in theory, simulations, and experiments [29,58–61]. Clearly, one would be tempted to relate our findings to this phenomenology of colloidal solutions; however, we showed that the origin of such effect in our case is different. For short range attractive colloidal systems at low temperature there is a glass phase originated solely by attraction and the reentrant melting arises from the competition between the high temperature and low temperature regime. For our system, however, there is no indication of an attraction dominated glass at low temperature and the destabilization of the glass is due to the destabilization of the cages that, in the high temperature regime, are responsible for the arrest. For $\eta \gtrsim 0.5$, we found that the glass-fluid line moves to higher densities when the temperature decreases. As a consequence, by increasing the intensity of the attraction, for a fixed density and arm number, the system moves from a liquid to a glass. This behavior is closely connected to the ultrasoft nature of the pair interaction. We recall that stars in a good solvent show a remelting of the glass phases (or solid phases at the equilibrium) for very high densities. The addition of attractive forces moves the glass-fluid line to higher densities. We could explain this effect as a contribution of the attraction to stabilize the cages and then to inhibit the remelting of the solution.

For $f=45,46$ the behaviors of $SP_2$ and $SP_3$ are very different. In the case $f=46$ for $SP_2$ we observed the qualitative behavior found for $f \geqslant 50$, while for $SP_3$ there exists a value of the temperature, $T^* \simeq 0.6$, below which the system does not present any sign of a glass transition. For $f=45$ considering $SP_2$ we observed the presence of a glass transition, while for the simply repulsive interaction this transition is not present for such value of $f$, i.e., the attraction seems to facilitate the formation of the glass. In the $SP_3$ case we did not observe glass phases for all the temperature values investigated. So in this case the effect of the addition of the attraction is a destabilization of the cages only.

To verify the MCT results we performed the analysis of the dynamics by means of MD simulations. As introduced in Sec. III A, the range of density which we examined is not sufficiently close to the ideal glass lines. For densities closer to the transition lines (mainly for $f=45,46$) the system shows a strong tendency toward crystallization. So we verify our MCT predictions for $f \geqslant 50$.

From the whole analysis performed, we evidenced a value of the packing fraction, i.e., $\eta=0.5$, which marks a change in the behavior of the solution. This value could be traced back to the crossover between the two different functional forms of the repulsion: the logarithmic form and the Yukawa one. For star polymers in a good solvent $\eta=0.5$, the so-called overlap packing fraction, corresponds to the packing fraction above which the radial distribution function shows a coordination shell inside the logarithmic core. In other words, for $\eta > 0.5$ stars start to interpenetrate widely. Also in this case the crossover designates approximatively the transition of the system through two different regimes. For $\eta < 0.5$ the response of the system to the introduction of attractive forces is a destabilization of the cage. This is mainly due to the change in the repulsive contribution at short distances which become softer and softer considering, respectively, $SP_1$, $SP_2$, and $SP_3$. For $\eta > 0.5$ stars interpenetrate more and more. The effect of the attraction seems to inhibit the remelting of the solution and the glass-fluid line move to higher densities. The shift of the transition line could be understood considering the effect of the attraction on the second shell of neighbors. Indeed, if we look the radial distribution function very close to the glass-fluid transition line, at low temperature, we observe that the second shell of particles is around $r=2$. In this region, see Fig. 1, we can observe that the system feels stronger attractive forces passing from $SP_1$ to $SP_2$ and then to $SP_3$. We conjecture that this attraction on the second neighbor shell is at the origin of the extended stabilized region of the glass phase for higher densities.

We must comment on some details relative to our analysis: first of all, $V_{\mathrm{tot}}$ does not present considerable repulsive maxima for large $r$ when the temperature is lower than $T^* \lesssim 1$ for $SP_2$ and $T^* < 0.8$ for $SP_3$. Obviously the repulsive contribution at longer range is more pronounced for higher temperatures (when the intensity of the attraction diminishes) and low arm numbers (when the Yukawa pair interaction decay to zero very slowly). Anyway, also below these temperatures, where the pair interaction shows a small repulsive contribution at large $r$ (around $\simeq 3$), we verify that our MCT predictions do not depend on the existence of the repulsive shoulder. Indeed we performed the same MCT calculation with a truncated potential in which the repulsive shoulder is suppressed. We conclude that for the temperature and densities of interest in our study the presence of this small repulsive contribution at large distance does not alter the picture of the glass regions. We emphasize that the presence of the shoulder is not an effect of our particular choice of the attractive contribution: due to the ultrasoft-core repulsion and to the Yukawa repulsive contribution at long range, the introduction of attractive forces of shorter range (i.e., depletion forces) could determine an additional repulsion outside the core.

Since the potential presents an ultrasoft-core interaction, it is difficult to determine a natural scale of energy (and length scale). We decided to rescale the temperature with respect to the integrated intensity of the attractive contribution ($T_{\mathrm{new}}$) in such a way to compare our results in a more significant way. In Fig. 14 we present a comparison between the MCT data obtained for $45 \leqslant f \leqslant 50$ considering the $SP_2$ and $SP_3$ models. As we can observe for $f=50$ the effect of destabilization of the cages as well as the inhibition of the melt is more accentuated for $SP_3$.

Finally, $SP_2$ and $SP_3$ show apparently conflicting behavior concerning $f=45,46$. Due to the very small range of $f$ it is very difficult to understand this peculiar behavior starting from the pair interaction. As we recall above, $\eta=0.5$ is a value for which star polymers in an athermal solvent, at the equilibrium, are in a solid phase and in particular 0.5 is just in the middle of the solid region ($34 < f < 70$). Around this region we find that the system has a very strong tendency to

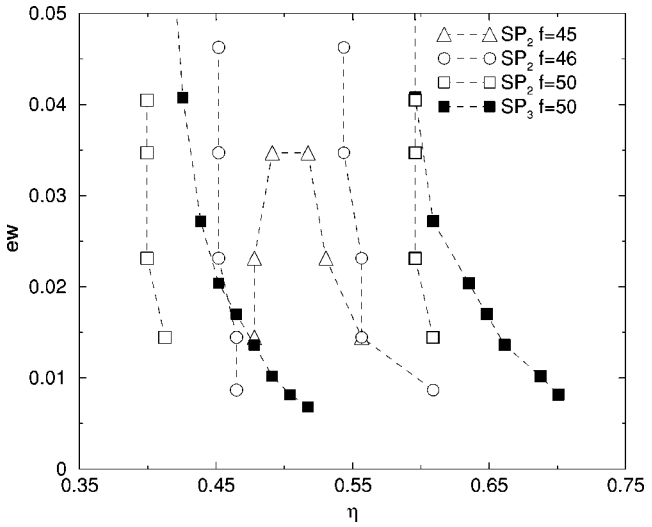


FIG. 14. Magnification of the low temperature MCT fluid-glass lines (computed with MHNC) for different $f$ values, $SP_2$, $SP_3$. The temperatures are rescaled with respect to the integrated intensity of the attractive contribution. Lines are simply a guide to the eye.

crystallize. Indeed, despite the change observed in the structure factor, and considering the connection between equilibrium phase diagram and glass transition line (Ref. [30]), we expect for $SP_2$ and $SP_3$ a small shift of the solid region with respect to the purely repulsive case. Note that this region corresponds to the glass region we determined for stars with $f=45,46$. It is not surprising that our data in the case of $f=45,46$ show an ambiguous trend between $SP_2$ and $SP_3$. For the above-mentioned reasons we do not believe it is very interesting to analyze further on $f \lesssim 46$.

We conclude from this analysis that the details of the phase diagram, concerning glass transition, is very sensitive to the particular, specific form of the attractive contribution. This could be mainly connected to the change of the short range repulsive contribution when attractive forces between stars are introduced and not dependent on the choice of the specific model. We expect the same behavior also considering depletion forces. Moreover, in the case of a general mixture of micelles with the hydrophobic group at the ends of the polymer chains, as discussed in Sec. II, the attractive contribution will be at very short range and close to interparticle separation equal to $\sigma$. This determines a change in a repulsive interaction in the region where in star polymer solution there is a crossover between the logarithmic form and the Yukawa one. We decide to complete our analysis considering a specific system described by specific attractive forces. Starting from this analysis, a future perspective of our work on star polymer solutions would be a more direct comparison between theory and experiments about the origin and the description of the attractive interaction. In this sense we decided to turn our attention, more in general, to systems of micelles which can be described by soft-core potential plus attraction at shorter range, similar to star polymer macromolecules. There exist many reasons to further study star polymer solutions: a precise understanding of their properties will allow the possibility of making progress in the exploration of hybrid polymeric-colloidal materials such as irregular multiarm stars, self-organized structures resulting from telechelic linear homopolymers and copolymers, polyelectrolyte brushes, and micelles with chemically fixed cores.

## ACKNOWLEDGMENTS

This work was funded in part by a grant from the Marie Curie program of the European Union, Contract No. MRTN-CT2003-504712. F.L.V. acknowledges financial support from INFM. G.F. and P.T. acknowledge financial support from MIUR-COFIN and MIUR-FIRB and thank Francesco Sciortino for useful discussions.

[1] The upper size limit of a colloidal particle is normally set at a radius of $1-2$ $\mu$m.
[2] R. J. Hunter, *Foundations of Colloid Science* (Oxford University Press, Oxford, 1987), Vol. 1.
[3] P. N. Pusey, in *Les Houches*, edited by J. P. Hansen, D. Levesque, and J. Zinn Justin (Elsevier, Amsterdam, 1948).
[4] C. N. Likos, S. Rosenfeldt, N. Dingenouts, M. Ballauff, P. Lindner, N. Werner, and F. Vögtle, J. Chem. Phys. **117**, 1869 (2002).
[5] P. G. Bolhuis, A. A. Louis, J. P. Hansen, and E. J. Meijer, J. Chem. Phys. **4**, 4296 (2001).
[6] G. S. Grest, L. J. Fetters, J. S. Huang, and D. Richter, Adv. Chem. Phys. **94**, 67 (1996).
[7] L.-L. Zhou and J. Roovers, Macromolecules **26**, 963 (1993).
[8] J. Roovers, L.-L. Zhou, P. M. Toporowski, M. van der Zwan, H. Iatrou, and N. Hadjichristidis, Macromolecules **26**, 4324 (1993).
[9] T. A. Witten and P. A. Pincus, Macromolecules **19**, 2509 (1986).
[10] M. Watzlawek, H. Löwen, and C. N. Likos, J. Phys.: Condens. Matter **10**, 8189 (1998).
[11] M. Watzlawek, C. N. Likos, and H. Löwen, Phys. Rev. Lett. **82**, 5289 (1999).
[12] B. Groh and M. Schmidt, J. Chem. Phys. **114**, 5450 (2000).
[13] W. D. Dozier, J. S. Huang, and L. J. Fetters, Macromolecules **24**, 2810 (1991).
[14] L. Willner, O. Jucknischke, D. Richter, J. Roovers, L.-L. Zhou, P. M. Oporowski, L. J. Fetters, J. S. Huang, M. Lin, and N. Hadjichristidis, Macromolecules **27**, 3821 (1994).
[15] C. N. Likos, H. Löwen, M. Watzlawek, B. Abbas, O. Jucknischke, J. Allgaier, and D. Richter, Phys. Rev. Lett. **80**, 4450 (1998).
[16] K. Ishizu, Prog. Polym. Sci. **23**, 1383 (1998).
[17] G. A. McConnell, A. P. Gast, J. S. Huang, and S. D. Smith, Phys. Rev. Lett. **71**, 2102 (1993).
[18] G. A. McConnell and A. P. Gast, Phys. Rev. E **54**, 5447 (1996).
[19] G. A. McConnell and A. P. Gast, Macromolecules **30**, 435

(1997).
[20] C. N. Likos and H. M. Harreis, Condens. Matter Phys. **5**, 173 (2002).
[21] J. Stellbrink, J. Allgaier, M. Monkenbush, D. Richter, A. Lang, C. N. Likos, M. Watzlawek, H. Löwen, G. Ehlers, and P. Schleger, Prog. Colloid Polym. Sci. **115**, 88 (2000).
[22] D. Vlassopoulos, G. Fytas, T. Pakula, and J. Roovers, J. Phys.: Condens. Matter **13**, R855 (2001).
[23] M. Kapnistos, D. Vlassopoulos, G. Fytas, K. Mortensen, G. Fleischer, and J. Roovers, Phys. Rev. Lett. **85**, 4072 (2000).
[24] B. Loppinet, E. Stiakakis, D. Vlassopoulos, G. Fytas, and J. Roovers, Macromolecules **34**, 8216 (2001).
[25] E. Stiakakis, D. Vlassopoulos, C. N. Likos, J. Roovers, and G. Meier, Phys. Rev. Lett. **89**, 208302 (2002).
[26] E. Stiakakis, D. Vlassopoulos, B. Loppinet, J. Roovers, and G. Meier, Phys. Rev. E **66**, 051804 (2002).
[27] W. Götze, in *Liquids, Freezing and Glass Transition*, edited by J. P. Hansen, D. Levesque, and J. Zinn-Justin (North-Holland, Amsterdam, 1991), p. 287.
[28] F. Sciortino, Nat. Mater. **1**, 145 (2002), News and Views.
[29] K. A. Dawson, Curr. Opin. Colloid Interface Sci. **7**, 218 (2002).
[30] G. Foffi, F. Sciortino, P. Tartaglia, E. Zaccarelli, F. Lo Verso, L. Reatto, K. A. Dawson, and C. N. Likos, Phys. Rev. Lett. **90**, 238301 (2003).
[31] F. Lo Verso, M. Tau, and L. Reatto, J. Phys.: Condens. Matter **15**, 1505 (2003).
[32] A. Parola and L. Reatto, Phys. Rev. A **31**, 3309 (1985).
[33] An ample review of HRT is contained in A. Parola and L. Reatto, Adv. Phys. **44**, 211 (1995).
[34] F. Barocchi, P. Chieux, R. Fontana, R. Magli, A. Meroni, A. Parola, L. Reatto, and M. Tau, J. Phys.: Condens. Matter **9**, 8849 (1997).
[35] A. N. Semenov, J.-F. Joanny, and A. R. Khokhlov, Macromolecules **28**, 1066 (1995).
[36] F. Laflécle, T. Nicolai, D. Durand, Y. Gnanou, D. Taton, Macromolecules **36**, 1341 (2003).
[37] F. Laflécle, D. Durand, and T. Nicolai, Macromolecules **36**, 1331 (2002).
[38] L. Fabbian, W. Götze, F. Sciortino, P. Tartaglia, and F. Thiery, Phys. Rev. E **59**, R1347 (1999).
[39] J. Bergenholtz and M. Fuchs, Phys. Rev. E **59**, 5706 (1999).
[40] K. A. Dawson, G. Foffi, M. Fuchs, W. Götze, F. Sciortino, M. Sperl, P. Tartaglia, T. Voigtmann, and E. Zaccarelli, Phys. Rev. E **63**, 011401 (2001).
[41] A. Puertas, M. Fuchs, and M. Cates, Phys. Rev. Lett. **88**, 098301 (2002).
[42] E. Zaccarelli, G. Foffi, K. A. Dawson, S. V. Buldyrev, F. Sciortino, and P. Tartaglia, Phys. Rev. E **66**, 041402 (2002).
[43] A. M. Puertas, M. Fuchs, and M. E. Cates, Phys. Rev. E **67**, 031406 (2003).
[44] G. Foffi, K. A. Dawson, S. V. Buldyrev, F. Sciortino, E. Zaccarelli, and P. Tartaglia, Phys. Rev. E **65**, 050802 (2002).
[45] F. Mallamace, P. Gambadauro, N. Micali, P. Tartaglia, C. Liao, and S.-H. Chen, Phys. Rev. Lett. **84**, 5431 (2000).
[46] K. N. Pham, A. M. Puertas, J. Bergenholtz, S. U. Egelhaaf, A. Moussad, P. N. Pusey, A. B. Schofield, M. E. Cates, M. Fuchs, and W. C. K. Poon, Science **296**, 104 (2002).
[47] T. Eckert and E. Bartsch, Phys. Rev. Lett. **89**, 125701 (2002).
[48] M. Daoud and J. P. Cotton, J. Phys. (Paris) **43**, 531 (1982).
[49] D. Richter, O. Jucknischke, L. Willner, L. J. Fetters, M. Lin, J. S. Huang, J. Allgaier, J. Roovers, C. Toporovski, and L.-L. Zhou, J. Phys. IV **3**, 3 (1993).
[50] J. Buitenhuis and S. Förster, J. Chem. Phys. **107**, 262 (1997).
[51] A. Jusufi, J. Dzubiella, C. N. Likos, C. von Ferber, and H. Löwen, J. Phys.: Condens. Matter **13**, 6177 (2001).
[52] F. Lado, S. M. Foiles, and N. W. Ashcroft, Phys. Rev. A **28**, 2374 (1983).
[53] J. P. Hansen and I. R. McDonald, *Theory of Simple Liquids* (Academic, London, 1986).
[54] F. Lado, S. M. Foiles, and N. W. Ashcroft, Phys. Rev. A **28**, 2374 (1983).
[55] L. Verlet and J.-J. Weis, Phys. Rev. A **5**, 939 (1972).
[56] The RY and MC results are obtained by Watzlawek *et al.*; see Ref. [10].
[57] F. J. Rogers and D. A. Young, Phys. Rev. A **30**, 999 (1984).
[58] K. N. Pham, A. M. Puertas, J. Bergenholtz, S. U. Egelhaaf, A. Moussad, P. N. Pusey, A. B. Schofield, M. E. Cates, M. Fuchs, and W. C. K. Poon, Science **296**, 104 (2002).
[59] A. M. Puertas, M. Fuchs, and M. E. Cates, Phys. Rev. Lett. **88**, 098301 (2002).
[60] F. Mallamace, P. Gambadauro, N. Micali, P. Tartaglia, C. Liao, and S.-H. Chen, Phys. Rev. Lett. **84**, 5431 (2000).
[61] T. Eckert and E. Bartsch, Phys. Rev. Lett. **89**, 125701 (2002).